OPEN JOURNAL SYSTEMS
ISSN:2237-2202

Available on line at Directory of Open Access Journals

Journal of Hyperspectral Remote Sensing v.04, n. 04 (2014) 100-110.

Journal of Hyperspectral Remote Sensing
www.ufpe.br/jhrs

ANALYSIS OF ENVIRONMENTAL PARAMETERS IN GILBUÉS – PI USING SATELLITE IMAGES

Élder Guedes dos Santos[1], Carlos Antonio Costa dos Santos[1] e Bergson Guedes Bezerra[2]

[1] Unidade Acadêmica de Ciências Atmosféricas, Centro de Tecnologia em Recursos Naturais, Universidade Federal de Campina Grande – UFCG, Av. Aprígio Veloso, 882, Bairro Universitário, Campina Grande – PB. Email: elder.ufcg@gmail.com; carlos@dca.ufcg.edu.br.
[2] Instituto Nacional do Semiárido – INSA, Campina Grande - PB. E-mail: bergson.bezerra@gmail.com.

Received October, 2013; revised February 2014; accepted May 2014.

ABSTRACT: This paper aims to analyze the desertification process in the Gilbués region, southwestern portion of Piauí state, through remote sensing techniques with a perspective of verify whether there is a relationship of environmental parameters (surface albedo, NDVI, surface temperature, radiation and energy balances, as well as non-evaporative fraction) with the desertification process presented in this study area. We used images from the satellite Landsat 5-TM of August 19, 1994 and August 15, 2010 and applied the SEBAL and S-SEBI algorithms for obtaining environmental parameters analyzed. It was diagnosed cover removal of native vegetation, which may indicate areas undergoing to desertification and/or environmental degradation. Similarly, there was a reduction of surface net radiation, increased soil heat fluxes, reduction of energy used for evaporation and increases in the energy used for heating the soil and air, causing the temperature increase, and a systematic increase of the soil moisture deficit in the studied region.
Keywords: Environmental degradation, remote sensing, SEBAL, S-SEBI

Introduction

Natural and anthropogenic changes are known to alter the surface energy balance and the hydrological cycle to different extents, which can produce regional effects and interfere in global weather patterns (Garcia et al., 2008). These events put pressure on ecosystems beyond resilience and cause degradation of the land. The UN Convention to Combat Desertification and Mitigate the Effects of Drought (UNCCD) conceptualizes the process of desertification as land degradation in arid, semiarid and dry subumid areas resulting from various factors such as climatic variations and human activities. It's linked to this concept the degradation of soil properties, vegetation and climate, which results in a persistent loss of ecosystem services that are critical to the maintenance of life (Pan - Brazil, 2004; D' Odorico et al, 2013). This process has important effects on the environment and societies, including soil erosion, reduction of vegetation cover, the change in composition of the plant community, or the loss of soil productivity, biodiversity and food security (D' Odorico et al. 2013). Desertification often leads to great social changes, including increased levels of poverty, hunger and rural exodus (Verstraete et al, 2009; D' Odorico et al, 2013.). According to the UNCCD, South America may take up to a fifth of their productive land affected by desertification, by the year 2025. Desertification has intensified in recent years, especially in countries with large tracts, such as Brazil and Argentina. The UN also estimates that about 30 % of Earth's land is affected by desertification (Carvalho, 2007).

The annual economic losses due to desertification reach 4 billion dollars throughout the world and 100 million dollars in Brazil alone. The problem is further aggravated by the fact that most of the regions affected by desertification being in poor areas in developing countries, such as Africa, where in the mid -1970s, 500,000 people died of hunger in the region known as the Sahel due to desertification (IICA , 2013).

The use of remote sensing is essential in studies of desertification, considering that offers the opportunity to acquire information of the spatial-temporal dynamics of this phenomenon. The information that can be produced with the sensor data provide support for decision making, such as prevention and rehabilitation of the affected lands. Thus, the evaluation of the affected process areas through remote sensing is important, considering that the delimitation of the area desertified allows action plans are developed to tackle the problem and prevent more areas are dominated by process (García et al , 2007; . 2008; Almeida -Filho and Carvalho , 2010).

The dry lands cover approximately 47 % of the land surface (Asner et al, 2003; . Lal , 2003) and General Circulation Models of the atmosphere (GCM) predict increased aridity occur related to global warming (Okin, 2002). About 35 % of the world population lives in regions subject to strong anthropogenic climate stress and pressures, which make them more vulnerable to land degradation. For these reasons, a better understanding of the relationships between these pressures and their effects on energy balance and water is relevant in these regions.

The relationship between the sensible heat fluxes (H) and latent heat (LE) of ecosystems is essential to quantify the water deficit of surface and to understanding of hydrological cycle. The law of conservation of energy shows that the available energy (Rn - G) to the surface is dissipated as latent and / or sensible heat, the partition of each depends on water availability (Garcia et al, 2007). The factors affecting this relationship include interactions between biogeochemical cycles, climate change, as well as interactions between plant physiology and the atmospheric boundary layer. An indicator of the surface water deficit, widely used, is the evaporative fraction (Λ). However, in semiarid areas, the evaporative latent heat and the fraction of natural vegetation are too low for several days, sometimes, with lower levels of sensitivity of sensing models to estimate values evaporation (<1 mm ET) (Garcia et al. , 2007). Therefore, this study not evaporative fraction (FNE = 1 - FE) will be used to evaluate the surface water deficit .

This study aims to analyze the process of desertification in the Gilbués municipality, in the southwestern of Piauí state, using remote sensing techniques, and to analyze the relationship between the parameters (surface albedo, NDVI, temperature surface, net radiation, soil heat flux, latent heat, sensible heat and not evaporative fraction) and desertification process presented in the studied region.

Materials and Methods

Study Area

Studies suggest that in NEB, greater than the Ceará state area was hit by desertification serious or very serious. The Ceará and Pernambuco states are the hardest hit, although proportionally, Paraíba is the state with the largest extent of the affected area, about 70 % of its territory already suffering from the effects of desertification (Figure 1a). The Brazilian semiarid region is the largest and most populous in the world, with almost 18 million inhabitants. Based on these problems, this study looks specifically at the core of Gilbués (PI) (Figure 1b) being the main causes of desertification core mining activities and extensive livestock and the consequent erosion processes that have their origin in the formation, genesis and morphology of their soils (Pan - Brazil , 2004; Perez - Marin et al , 2012.).

a)

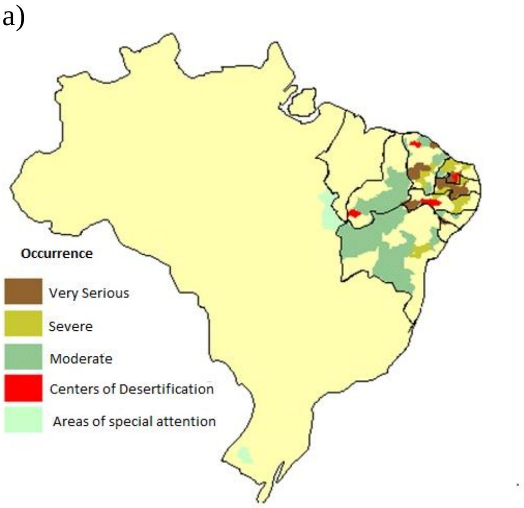

b)

Figure 1: a) Centers of desertification in northeast Brazil (MMA, 2013) b) affected by the degradation process in the environs of the Gilbués-PI city (Carvalho, 2007) area.

Data

For this study TM satellite images were used - Landsat 5 in orbit 220, point 67, the dates August 19, 1994 and August 15, 2010 acquired the catalog of images of the Imaging Division (DGI) of the National Institute for Space Research (INPE) through the website (http://www.dgi.inpe.br). The criterion for the choice of images was minimal cloud cover, since they can bring errors to the results. These two years studied were chosen because they present images without the presence of clouds in the same month (August), and are years with similar climatic behavior.

Methodology

The image processing was done using ERDAS Imagine 8.5 software. To obtain the parameters albedo, vegetation indices, surface temperature, net radiation, energy balance and evaporative fraction of the SEBAL and S - SEBI algorithms were used. Such algorithms are described below.

The computational steps to obtain the components of the net radiation through the SEBAL algorithm are shown in the flowchart of Figure 2 and detailed in the following.

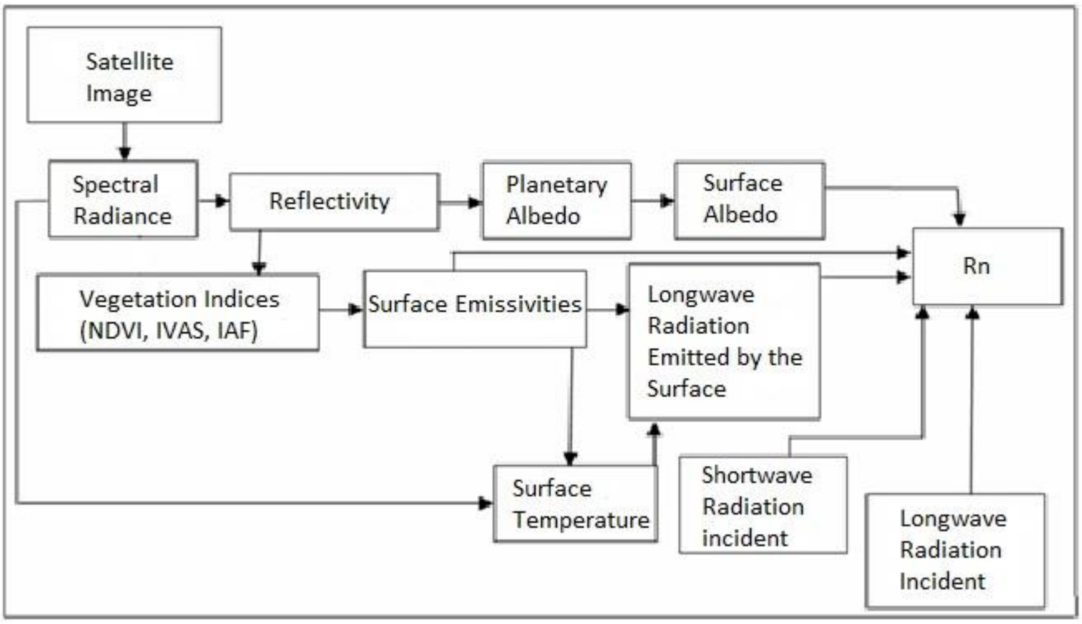

Figure 2: Flowchart of steps for obtaining the surface net radiation (Rn) by SEBAL algorithm.

The first computational stage of SEBAL is to obtain radiometric calibration or spectral radiance (L_λ), which is calculated as follows :

$$L_\lambda = \left(\frac{L_{MAX} - L_{MIN}}{255}\right) DN + L_{MIN} \quad (1)$$

where DN is the digital number of each pixel of the image, L_{MAX} and L_{MIN} are calibration constants of the spectral sensor, the values for the Landsat TM-5 are described in Chander and Markham (2003).

Then we calculate the monochromatic reflectance (ρ_λ), which is the ratio of reflected solar radiation incident on each pixel. In other words ρ_λ represents the portion of solar radiation that is reflected from each band. Its calculation is obtained by the following equation (Allen et al, 2002.)

$$\rho_\lambda = \frac{\pi L_\lambda}{ESUN_\lambda \cos\theta d_r} \quad (2)$$

where L_λ is the spectral radiance; $ESUN_\lambda$ is the monochromatic solar constant associated with each band TM - Landsat 5, whose values are described in Chander and Markham (2003); θ is the zenith angle of the sun and d_r is the relative distance Earth-Sun, which is obtained by Equation 3.

$$d_r = 1 + 0{,}033\cos\left(DOA\frac{2\pi}{365}\right) \quad (3)$$

where *DOA* is order day of the year in order that the radiometric data (satellite images) are obtained, whose values correspond to the days of the generation of images.

Calculating the albedo at the top of the atmosphere (α_{toa}) is made by a linear combination of the spectral reflectance (ρ_λ), calculated previously and the weights (ϖ_λ) that for each band, and are given by:

$$\alpha_{toa} = (\varpi_1\rho_1) + (\varpi_2\rho_2) + (\varpi_3\rho_3) + (\varpi_4\rho_4) + (\varpi_5\rho_5) + (\varpi_7\rho_7) \quad (4)$$

The coefficients (ϖ_1, ϖ_2,... ϖ_7) of the previous equation for the Landsat TM-5, are described in Allen et al. (2002).

The albedo of the surface albedo or corrected to atmospheric effects, which is a first term of the radiation balance, is computed using the following equation:

$$\alpha = \frac{\alpha_{toa} - \alpha_{path\_radiance}}{\tau_{sw}^2} \quad (5)$$

where α_{toa} is the planetary albedo $\alpha_{path\_radiance}$ is the portion of the solar radiation reflected by the atmosphere (Bastiaanssen, 2000) and τ_{sw} is the atmospheric transmissivity, which is defined as the fraction of incident solar radiation is transmitted through the atmosphere and its effect absorption and reflection (Allen et al. 2002). The atmospheric transmissivity is computed depending on the local altitude (z), in meters, according to the equation:

$$\tau_{sw} = 0{,}75 + 2\times10^{-5} z \quad (6)$$

Normalized Difference Vegetation Index (NDVI), which is indicative of the conditions of density and height of vegetation, is obtained by the ratio between the difference of near infrared reflectance (ρ_4) and red (ρ_3) and the sum the same reflectance as the equation:

$$NDVI = (\rho_4 - \rho_3)/(\rho_4 + \rho_3) \quad (7)$$

The Soil Adjusted Vegetation Index (SAVI) is a vegetation index that aims to alleviate the effects of “background " soil, being obtained by the equation proposed by Huete (1988):

$$SAVI = (1+F)(\rho_4 - \rho_3)/(F + \rho_4 + \rho_3) \quad (8)$$

where F is a soil adjustment factor (F = 0.5) (Allen et al . , 2007a).

The computation of Leaf Area Index (LAI), which is the ratio between the total area of all leaves contained in a given pixel, the pixel area is done by empirical equation obtained by Allen et al. (2002)

$$IAF = -\frac{\ln\left(\frac{0{,}69 - SAVI}{0{,}59}\right)}{0{,}91} \quad (9)$$

The calculation of the surface temperature is made by the Planck equation inverted proposal for a black body to which the emissivity is equal to 1. Since each pixel is not a black body there is a need to establish its emissivity in the field the thermal spectral band (ε_{NB}), for purposes of computation of Ts as well as in the computation of long wave radiation emitted by the surface , which in this case is considered broadband emissivity(ε_0) (4 – 100 µm).

The computation of both emissivity is done by the following equations, according to the IAF (Allen et al, 2002.)

$$\varepsilon_{NB} = 0{,}97 + 0{,}00331 IAF \quad (10a)$$

$$\varepsilon_0 = 0{,}95 + 0{,}01 IAF \quad (10b)$$

ε_{NB} = ε_0= 0,98 are considered when LAI ≥ 3 and NDVI < 0 , in the case of bodies of water, it is considered ε_{NB} = 0,99 e ε_0= 0,985, according to the proposal of Allen et al. (2002).

Obtaining T_s, as previously mentioned, is made by the Planck equation reversed, depending on the spectral radiance of thermal band $L_{\lambda,6}$ and emissivity obtained by equation (11a) :

$$T_s = \frac{K_2}{\ln\left(\frac{\varepsilon_{NB} K_1}{L_{\lambda,6}} + 1\right)} \quad (11)$$

where K1 = 607.8 W m - 2 sr- 1 mM - 1 and K2 = 1261 K.

The third term of the radiation balance is calculated by SEBAL the flow of thermal radiation emitted by the surface. Its computation is done by the Stefan-Boltzmann equation, as a function of temperature and surface emissivity, which is:

$$R_{L\uparrow} = \varepsilon_0 \sigma T_s^4 \quad (12)$$

Where σ is Boltzmann constant (5.67 × 10 8 W m -2 K -4) and the other terms have been previously defined.

The longwave radiation emitted by the atmosphere toward the surface (W m - 2) is also calculated by the Stefan- Boltzmann equation, depending on the emissivity of air is obtained from equation (16) and air temperature (Ta) , obtained from a meteorological station in the study area :

$$R_{L\downarrow} = \varepsilon_a \sigma T_a^4 \quad (13)$$

The emissivity of air (ε_a) is obtained by:

$$\varepsilon_a = 0{,}85(-\ln \tau_{sw})^{0{,}09} \quad (14)$$

The second term of the radiation balance is the radiation incident short wave, which is calculated by the following equation :

$$R_{s\downarrow} = G_{sc} \cos\theta d_r \tau_{sw} \quad (15)$$

where G_{sc} is the solar constant (1367 W m^{-2}) and the other terms have been previously defined .

The SEBAL makes the computation of Rn by the equation:

$$R_n = R_{S\downarrow} - \alpha . R_{S\downarrow} + R_{L\downarrow} - R_{L\uparrow} - (1-\varepsilon_0)R_{L\downarrow} \quad (16)$$

where is the short or solar radiation incident wave (W m - 2) , the term is the portion of the shortwave radiation reflected by the surface (W m - 2) is the surface albedo , is the longwave radiation emitted through the atmosphere toward the surface (W m - 2) , is the longwave radiation emitted by the surface (W m^{-2}); $(1-\varepsilon_0)R_{L\downarrow}$ the term corresponding to long wave radiation reflected and ε_0 is the surface emissivity .

The G value is computed by Bastiaanssen (2000):

$$G = \left[\frac{T_s}{\alpha}\left(0{,}0038\alpha + 0{,}0074\alpha^2\right)\left(1 - 0{,}98 NDVI^4\right)\right] R_n$$
(17)

Where T_s is surface temperature (ºC), α is surface albedo, NDVI is vegetation index and R_n is net radiation (W m^{-2}).

The steps of S-SEBI algorithm to estimate of sensible heat flux (H) and latent flux, evaporative fraction (Λ) (Sobrino et al., 2005) are write below and evaporative fraction for each pixel with reflectance α_0 and temperature T_0 was obtained by Roerink et al., 2000; Sobrino et al., 2007:

The evaporative fraction (Λ) was calculated by:

$$\Lambda = \frac{T_H - T_0}{T_H - T_{LE}} \quad (18)$$

The Figure 3 shows the spatial characteristics of the surface reflectance and surface temperature together with the average reflectance per unit temperature. Spatial distribution is possible to recognize the lower limit, where the latent heat flux is assumed to be maximum $LE_{max}(\alpha_0)$ and the upper limit located where the sensible heat flux is maximum $H_{max}(\alpha_0)$ (Sobrino et al., 2005; Gómez et al., 2005; Santos e Silva, 2008). The linear equation representing the maximum and minimum values can be written as:

$$T_H = a_H + b_H \alpha_0 \quad (19)$$

and

$$T_{LE} = a_{LE} + b_{LE} \alpha_0 \quad (20)$$

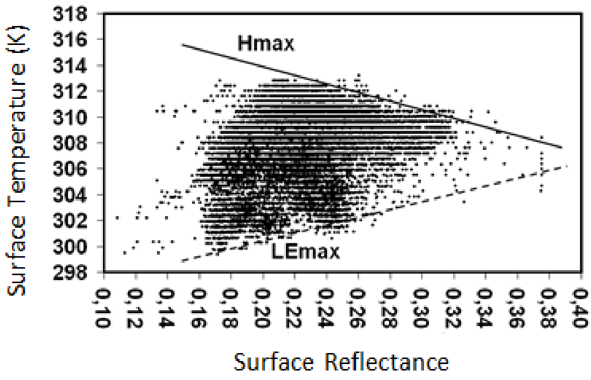

Figure 3: Schematic representation of the relationship between the surface temperature and the surface reflectance.

The regression variables and are local and temporal.

Replacing the relationship observed by T_H e T_{LE}, the evaporative fraction is written as:

$$\Lambda = \frac{a_H + b_H \alpha_0 - T_0}{a_H - a_{LE} + (b_H - b_{LE})\alpha_0} \quad (21)$$

Once you determine the Λ, the sensible heat flux (H) and latent heat flux (LE) will be calculated as described below (Santos e Silva, 2008):

$$H = (1-\Lambda)(R_n - G) \quad (22)$$

$$LE = \Lambda(R_n - G) \quad (23)$$

To obtain the Not Evaporative Fraction (*FNE*) the following equation was used, as proposed by Garcia et al. (2007):

$$FNE = 1 - \Lambda = 1 - \frac{LE}{LE + H} = 1 - \frac{LE}{(R_n - G)} = \frac{H}{(R_n - G)} \quad (24)$$

Results and Discussion

Figure 4a shows the distribution of NDVI on August 19, 1994, it is observed that the areas that are in shades of green are the corresponding vegetated areas, with values ranging between 0.45 and 0.60 mostly. The red and brown shades represent areas of exposed soil and urban areas, with values between 0.01 and 0.30. The same analysis of NDVI was performed for the date August 15, 2010 (Figure 4b), however it was observed that there was a growth in areas with low values of NDVI, which is associated with areas where there has been the removal of native vegetation cover that may indicate areas of desertification and / or environmental degradation process.

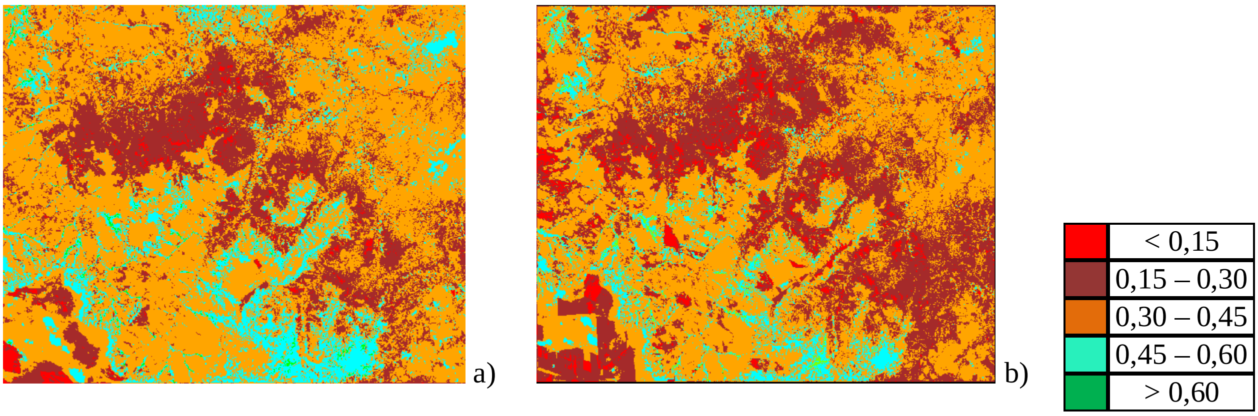

Figure 4: Spatial distribution of NDVI in Gilbués-PI in days a) 08/19/1994 e b) 08/15/2010.

The surface albedo exerts a control on the amount of energy that is absorbed by Earth's surface, directly affecting the bottom line of radiation and energy. Figure 5 shows the spatial distribution of surface albedo on August 19, 1994 (Figure 4a) and 15 August 2010 (Figure 4b). It is noticed that the areas with the lowest values of the albedo between 0.04 and 0.09 are related to areas of higher values of NDVI (Figures 5a and 5b) . This inverse relationship between NDVI and albedo is due to the high rate of radiation that is absorbed by vegetation which is used in bio physicochemical sues processes such as breathing and perspiration. Thus, the portion of the radiation that is reflected into the atmosphere is low. When the vegetation is removed and the soil is thus exposed, the rate of absorption of solar radiation is low, given that these processes are bio physicochemical drastically reduced. As a result, high levels of energy are lost by surface reflectivity. This behavior is observed in the areas of bare soil NDVI values are lower than the 0.3 albedo values varying in the range between 0.19 and 0.42 for the day August 19, 1994 (Figure 5a). In the same areas, but on August 15, 2010, the albedo ranged from 0.26 to 0.50 (Figure 5b). This increase in the range of variation observed in the same areas is probably indicative of the expansion of the loss of ground cover, making it exposed to solar radiation, which is indicated by the high reflectivity.

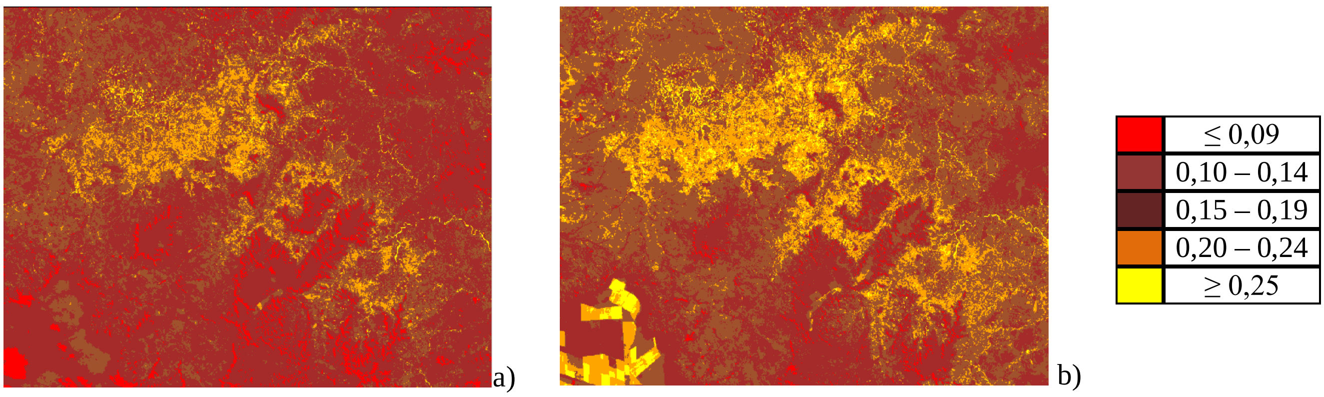

Figure 5: Spatial distribution of albed in Gilbués-PI in days a) 08/19/1994 e b) 08/15/2010.

In Figure 6, which corresponds to the spatial distribution of the surface temperature in 1994 and 2010 (Figure 6a and Figure 6b, respectively), it appears that in areas with low rates of vegetation, the temperature increased in the range of 0.1 at 4 ° C. As there is the distance of these vegetated areas and the approach towards the area of desertification process, this temperature difference increases, reaching values greater than 4 ° C. These values can be explained due to the fact that the vegetation transpires, releases water vapor and increases the humidity in its surroundings, the softening temperature of the locations that are close to this area, unlike in the area affected by desertification which have a lower wooded area which is a direct consequence of human interference in nature, which contribute to increased temperature, or heat sensitive release to the atmosphere.

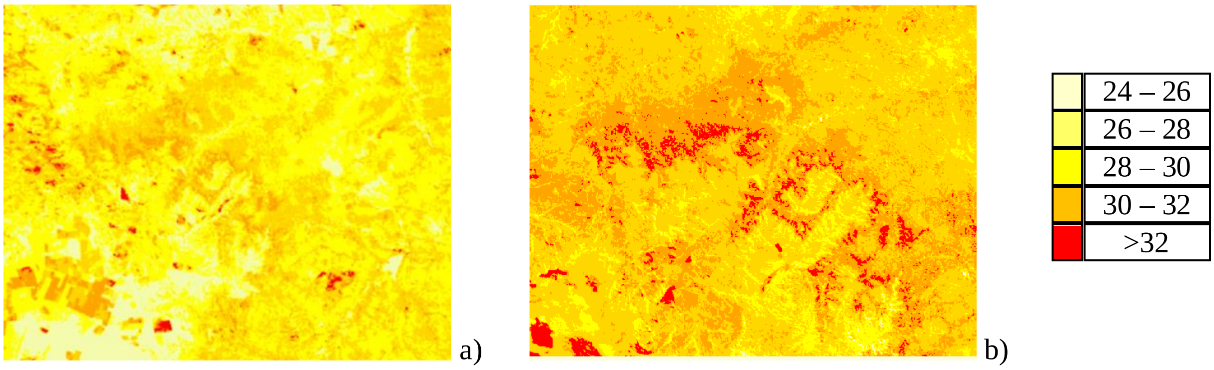

Figure 6: Spatial distribution of surface temperature (Ts) in Gilbués-PI in days a) 08/19/1994 e b) 08/15/2010.

The ability of vegetation to modify some attributes such as surface albed, roughness, soil moisture, surface temperature, etc. Which are crucial in the quantification of the rate of energy flows to the surface, is mentioned by D' Odorico et al. (2013) as one of the main types of feedback from global desertification. The removal of vegetation and the consequent exposure of the soil surface to erosion from wind and water cause significant losses of soil nutrients, thereby preventing the re-establishment of vegetation (Schlesinger et al, 1990; . D' Odorico et al, 2013). According to D' Odorico et al. (2013) this type of feedback relies on the ability of vegetation to stabilize the soil surface as the mechanism that allows the system persists in a vegetated or bare soil condition.

The spatial distribution of net radiation (Rn) (W m^{-2}), August 19, 1994, shown in Figure 7a, it is seen that the highest values in Rn are found in areas with vegetation and water bodies, range 550-600 W m^{-2} and greater than 600 W m^{-2}. In areas with exposed soil is Rn with values between 450-490 W m^{-2}, a fact that may be explained by human activities, causing an increase in the reflectivity of those areas. In Figure 7b it is found southwest of the image increased net radiation with a range of approximately 100 W m^{-2}, this variation can be explained by the use of these areas for agricultural purposes in the area of desertification process is observed a decrease in NB that is related to the removal of native vegetation (thus increasing the area of bare ground), causing an increase in the amount of energy incident on the ground.

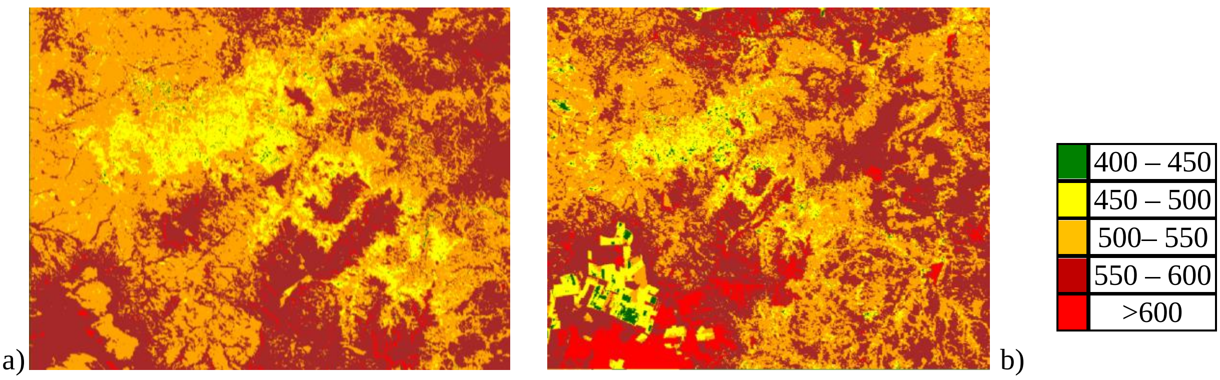

Figure 7: Spatial distribution of net radiation (Rn) in Gilbués-PI in days a) 08/19/1994 e b) 08/15/2010.

In the spatial distribution of heat flow on the ground (G) Figure 8, amounts are ranging from less than 50 W m^{-2} and greater than 80 W m^{-2}. The lowest values are in the areas of vegetation that has greater ground cover and hence there is a lower incidence of direct solar radiation at ground level. The highest values are in areas where desertification and regions devoid of vegetation, around 90 to 100 W m^{-2} process. It is noted also an increase in G in Figure 8b with respect to Figure 8a, this motif related to the removal of native vegetation and irregular use of the soil.

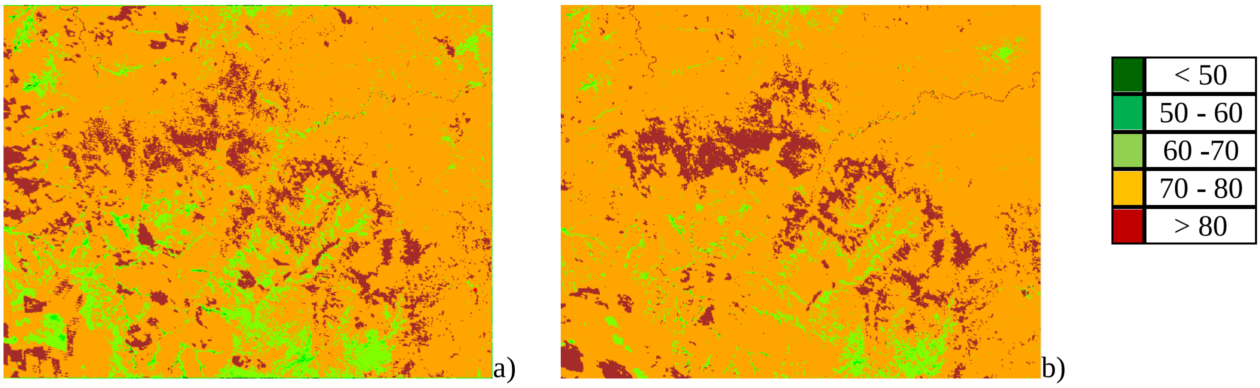

Figure 8: Spatial distribution of soil heat flux (*G*) in Gilbués-PI in days a) 08/19/1994 e b) 08/15/2010.

The sensible heat flux (H) (Figure 9) shows values ranging from less than 100 W m^{-2} and 500 W m^{-2}. It is observed that in areas where there were low values of H (Figure 9a) there was a considerable increase (Figure 9b), through a relationship with NDVI is perceived that this was due to removal of native vegetation. The replacement of vegetated areas by areas of bare soil results in a decrease in energy used for evaporation and increases the energy used to heat the soil and air, causing the temperature increase. The lowest values of H are shown in vegetated areas, where most of the energy is used in the evapotranspiration process.

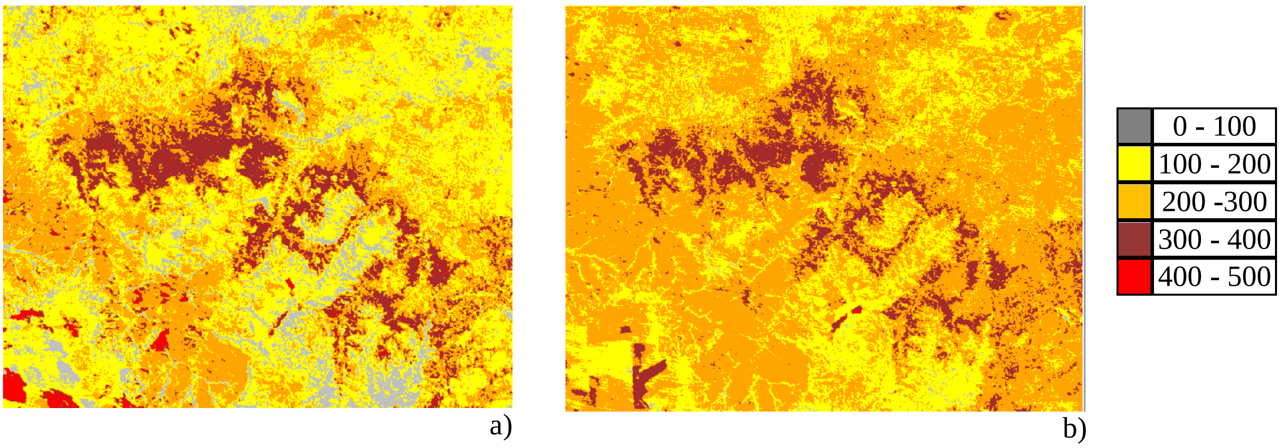

Figura 9: Spatial distribution of sensible heat flux (*H*) in Gilbués-PI in days a) 08/19/1994 e b) 08/15/2010.

Figure 10a shows the spatial distribution of the latent heat (LE) on August 19, 1994 . Values of LE varies mostly between 200 W m^{-2} and 400 W m^{-2}. From Figure 10b, ie , the spatial distribution of latent heat in August 15, 2010 , one can observe that areas with low values were expanded, this indicates that the reduction in vegetation at the core of desertification in Gilbués-PI, which can exacerbate even further the process of desertification and / or environmental degradation. The values of the LE range, mostly between 100 W m^{-2} and 500 W m^{-2}. The highest values of LE are shown on areas of vegetation and water. Most of the energy is used in evaporation and evaporation process, respectively. The lowest values of LE are the areas that present the removal of native vegetation for use of mining and ranchers activities. The results found in this study are in agreement with those found by Ma et al. (2002) have obtained the spatial distributions for the flow of energy to the surface using satellite remote sensing for the region in the process of desertification in northwestern China .

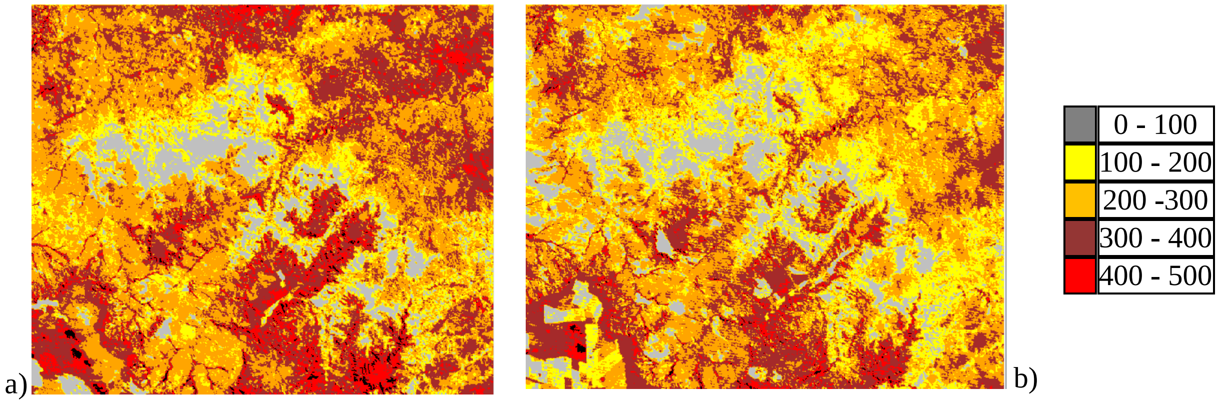

Figure 10: Spatial distribution of the latent flux (*LE*) in Gilbués-PI in days a) 08/19/1994 e b) 08/15/2010.

Comparing Figure 11a represents the spatial distribution of non-evaporative fraction (FNE), on August 19, 1994, with Figure 11b, which represents the spatial distribution of FNE, on August 15, 2010, observed that areas increased considerably red in color, indicating that there was an increase of water deficit in soil over the years. This is due to the fact that the natural vegetation has been removed, as evidenced by the NDVI (see Figures 5a and 5b) and, thus, a greater soil exposure to sunlight, leading to an increase in the rate of evaporation thereof. In addition, the surface temperature is also reported an increase of approximately 2 ° C in this area as well as a greater amount of energy being absorbed by the soil (greater heat flow in the soil in this area).

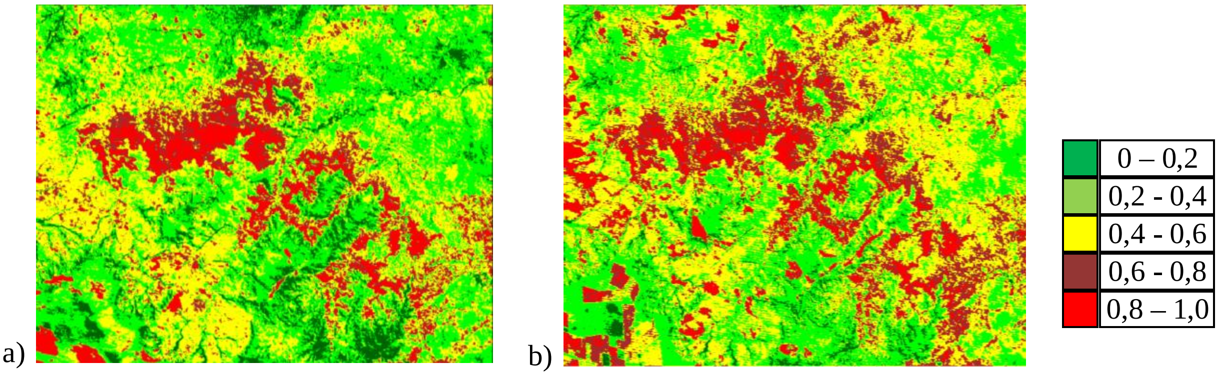

Figure 11: Spatial distribution of evaporative fraction (*FNE*) in Gilbués-PI in days a) 08/19/1994 e b) 08/15/2010.

These results are worrying because all environmental parameters, whose spatial distribution was obtained by orbital images of high spatial resolution (30m) indicated an increased degree of environmental degradation, specifically the vegetation, the Center for Desertification Gilbués - PI, that this area can lead to irreversible degradation process.

Ceprani et al. (2004) state that , in the Center for Desertification Gilbués, the native vegetation is succeeded by a grass cover, known locally as " mottled", unable to perform efficiently the task of protecting the soil surface against the high levels of rainfall intensity, characterized by heavy rains and short-lived , with over 500 mm / month that strike annually over the region , and the grooves index, first developed in the area covered by grasses , succeed gullies that destroy all soil horizons exposing finally, pellites constituting the bedrock.

According to Carvalho (2007) can be stated that if the rainfall in arid, semi-arid and dry sub-humid regions have greatly influenced the process of desertification on vegetation and, therefore, studies in different seasons are needed to increase the accuracy and reliability of the final result.

Conclusions

From the results obtained and discussed above, it was possible to reach the following conclusions:

1) an increase in areas with low values of NDVI, which is associated with areas where there has been the removal of native vegetation cover, which may indicate areas of desertification and /

or environmental degradation process was observed.

2) It was found that in areas with low vegetation indices, the temperature increased in a range of 0.1 to 4 ° C and, as there is the distance of these vegetated areas and the approach towards the area of desertification and / or environmental degradation , this difference reaches values higher than 4 ° C.

3) In areas of desertification , reduction of net radiation at the surface and an increase in heat flow in the soil , which is related to the increasing areas of exposed soil was observed. Similarly, replacement of vegetated areas by areas of bare soil resulted in a decrease in energy used for evaporation and increases the energy used to heat the soil and air, causing the temperature increase.

4) During the period studied, based on satellite images and the algorithms used, we observed a systematic increase in the moisture deficit in the soil of the region studied.

Acknowledgments

The authors thanks CNPq by scolarship to firts author. Project, N°. 562424/2010-5, Edital 35/2010.

References

Allen, R.; Tasumi, M.; Trezza, R. 2002. SEBAL (Surface Energy Balance Algorithms for Land) – Advanced Training and Users Manual – Idaho Implementation, version 1.0.

Almeida-Filho, R.; Carvalho, C. M. 2010. Map ping land degradation in the Gilbués region, northeastern Brazil, using Landsat TM images. International Journal of Remote Sensing, v. 31, p. 1087–1094.

Asner, G. P.; Borghi, C. E.; Ojeda, R. A. 2003. Desertification in Central Argentina: changes in ecosystem carbon and nitrogen from imaging spectroscopy. Ecological Applications, v.13, p.629−648.

Bastiaanssen, W. G. M. 2000. SEBAL-based sensible and latent heat fluxes in the irrigated Gediz Basin, Turkey. Journal of Hydrology, v. 229, p. 87-100.

Carvalho, C. M. 2007. Avaliação da desertificação no Sudoeste do Estado do Piauí- PI, através de técnicas de sensoriamento remoto. São Jose dos Campos: INPE.

Chander, G.; Markham, B. 2003. Revised Landsat-5 TM Radiometric Calibration Procedures and Post calibration Dynamic Ranges. IEEE Transactions on Geoscience and Remote Sensing, v. 41, p. 2674-2677.

Crepani, E.; Medeiros J.S. De; Palmeira, A.F. 2004. Intensidade pluviométrica: uma maneira de tratar dados pluviométricos para análise da vulnerabilidade de paisagens à perda de solo. São José dos Campos: INPE, ago. 30 p. (INPE-11237-RPQ/760).

D’odiorico, P.; Bhattachan, A.; Davis, K. F.; Ravi, S.; Runyan, C. W. 2013. Global desertification: Drivers and feedbacks. Advances in Water Resources, v.51, p.326-344.

García, M.; Villagarcía, L.; Contreras, S.; Domingo, F.; Puigdefábregas, J. 2007. Comparison of Three Operative Models for Estimating the Surface Water Deficit using ASTER Reflective and Thermal Data. Sensors, v.7, p.860-883.

Huete, A. R. 1988. A soil adjusted vegetation index – SAVI. Remote Sensing of Environment, v. 25, p. 295–309.

IICA, 2013. Instituto Interamericano de Cooperação para a Agricultura, 2013. Disponível em: http://www.iicadesertification.org.br/ Acesso em: 23/03/2013.

LAL, R. 2003. Carbon Sequestration in Dryland Ecosystems. Environmental Management, v.33, n.4, p.528-544.

Ma, Y.; Tsukamoto, O.; Hirohiko, I. 2002. Remote sensing parameterization of the processes of energy and water cycle over desertification areas. Science in China (Series D), v. 45 Supp., p. 47-53.

Okin, G. S. 2002.Toward a unified view of biophysical land degradation processes in arid and semi-arid lands. In J. F. Reynolds; D. M. Stafford Smith (Eds.), Global Desertification: Do Humans Cause Deserts? p. 95−109, Berlin, Dahlem University Press.

Pan-Brasil. 2004. Ministério do Meio Ambiente. Secretaria de Recursos Hídricos. Programa de Ação Nacional de Combate à Desertificação e Mitigação dos Efeitos da Seca: PAN – Brasília.

Perez-Marin, A. M.; Cavalvante, A. M. B.; Medeiros, S. S.; Tinôco, L. B. M.; Salcedo, I. H. 2012. Núcleos de desertificação no semiárido brasileiro: ocorrência natural ou antrópica? Parcerias Estratégicas, v.17, n.34, p.87-106.

Roerink, G. J.; Su, Z.; Menenti, M. 2000. A Simple Remote Sensing Algorithm to Estimate the Surface Energy Balance. Physics and Chemistry of the Earth (B), v. 25, p. 147-157.

Santos, C. A. C.; Silva, B. B. 2008. Estimativa da evapotranspiração da bananeira em região semiárida através do algoritmo S-SEBI. Revista Brasileira de Agrometeorologia, v. 16, p. 9-20.

Schlesinger, W. H.; Reynolds, J. F.; Cunningham, G. L.; Huenneke, L. F.; Jarreli, W. M.; Virginia, R. A.; Whitford, W. G. 1990. Biological Feedbacks in Global Desertification. Science, v.247, p.1043-1048.

Sobrino, J. A.; Gomez, M.; Jimenez-Munoz, J. C.; Olioso, A. 2007. Application of a simple algorithm to estimate daily evapotranspiration from NOAA-AVHRR images for the Iberian Peninsula. Remote Sensing of Environment, v. 110, p. 139-148.

Sobrino, J. A.; Gomez, M.; Jimenez-Munoz, J. C.; Olioso, A.; Chehbouni, G. 2005. A simple algorithm to estimate evapotranspiration from DAIS data: Application to the DAISEX Campaigns. Journal of Hydrology, v. 315, p. 117−125.

Sobrino, J. A.; Jacob, F. 2005. Retrieval of evapotranspiration over the Alpilles/ReSeDA experimental site using airborne POLDER sensor and thermal camera. Remote Sensing of Environments, v. 96, p. 399-408.

Verstraete, M. M.; Scholes, R. J.; Smith, M. S. 2009. Climate and desertification: looking at an old problem through new lenses. Frontiers in Ecology and the Environment, v.7, p.421–428.